Evidence for a Multipolar Magnetic Field in SGR J1745-2900 from X-Ray Light-curve Analysis

Rafael C. R. de Lima[1,2] , Jaziel G. Coelho[2,3,4] , Jonas P. Pereira[5,6,7] , Claudia V. Rodrigues[4] , and Jorge A. Rueda[2,8,9,10,11]

[1] Universidade do Estado de Santa Catarina, Av. Madre Benvenuta, 2007 Itacorubi, 88.035-901, Florianópolis, Brazil; rafael.lima@udesc.br
[2] ICRANet, Piazza della Repubblica 10, I-65122, Pescara, Italy; jazielcoelho@utfpr.edu.br
[3] Departamento de Física, Universidade Tecnológica Federal do Paraná, 85884-000 Medianeira, PR, Brazil
[4] Divisão de Astrofísica, Instituto Nacional de Pesquisas Espaciais, Avenida dos Astronautas 1758, 12227-010, São José dos Campos, SP, Brazil
[5] Universidade Federal do ABC, Centro de Ciências Naturais e Humanas, Avenida dos Estados, 5001-Bangú, CEP 09210-170, Santo André, SP, Brazil
jpereira@camk.edu.pl
[6] Mathematical Sciences and STAG Research Centre, University of Southampton, Southampton, SO17 1BJ, UK
[7] Nicolaus Copernicus Astronomical Center, Polish Academy of Sciences, Bartycka 18, 00-716, Warsaw, Poland
[8] ICRANet-Rio, Centro Brasileiro de Pesquisas Físicas, Rua Dr. Xavier Sigaud 150, 22290-180 Rio de Janeiro, Brazil
[9] ICRANet-Ferrara, Dipartimento di Fisica e Scienze della Terra, Università degli Studi di Ferrara, Via Saragat 1, I-44122 Ferrara, Italy
[10] Dipartimento di Fisica e Scienze della Terra, Università degli Studi di Ferrara, Via Saragat 1, I-44122 Ferrara, Italy
[11] INAF, Istituto di Astrofisica e Planetologia Spaziali, Via Fosso del Cavaliere 100, I-00133 Rome, Italy

Abstract

SGR J1745-2900 was detected from its outburst activity in 2013 April and it was the first soft gamma repeater (SGR) detected near the center of the Galaxy (Sagittarius A*). We use 3.5 yr *Chandra* X-ray light-curve data to constrain some neutron star (NS) geometric parameters. We assume that the flux modulation comes from hot spots on the stellar surface. Our model includes the NS mass, radius, a maximum of three spots of any size, temperature and positions, and general relativistic effects. We find that the light curve of SGR J1745-2900 could be described by either two or three hot spots. The ambiguity is due to the small amount of data, but our analysis suggests that one should not disregard the possibility of multi-spots (due to a multipolar magnetic field) in highly magnetized stars. For the case of three hot spots, we find that they should be large and have angular semiapertures ranging from 16° to 67°. The large size found for the spots points to a magnetic field with a nontrivial poloidal and toroidal structure (in accordance with magnetohydrodynamics investigations and *Neutron Star Interior Composition Explorer*'s (*NICER*) recent findings for PSR J0030+0451) and is consistent with the small characteristic age of the star. Finally, we also discuss possible constraints on the mass and radius of SGR J1745-2900 and briefly envisage possible scenarios accounting for the 3.5 yr evolution of SGR J1745-290 hot spots.

Key words: dense matter – pulsars: general – stars: neutron – starspots – X-rays: individual (SGR J1745-2900)

1. Introduction

Electromagnetic data-driven constraints to the mass and radius of NSs are very elusive. Radius measurements are mostly based on the observation of thermal emission and comparisons with theoretical models. The modeling, however, due to the complex and relativistic nature of NSs, suffers from a number of complications such as parameter degeneracy, the unknown NS equation of state (EOS), among other uncertainties, e.g., the distance to the object (see, e.g., Özel et al. 2016b; Özel & Freire 2016, and references therein). Notwithstanding, currently operating and future observatories, such as the *Neutron Star Interior Composition Explorer* (*NICER*; Gendreau et al. 2016), the enhanced X-ray Timing and Polarimetry mission (Zhang et al. 2019), and the Spectroscopic Time-Resolving Observatory for Broadband Energy X-rays (Ray et al. 2018), promise to greatly decrease the uncertainties of NS parameters. They are expected to provide masses and radii of NSs with an accuracy of a few percent (see Sieniawska et al. 2018, and references therein). In particular, one of the most significant developments in the measurement of the dense matter EOS is going to come from the *NICER* detector (see Özel et al. 2016a). The pulsed X-ray emission from hot spots on the surface of a rotating NS contains encoded information about its gravitational field and the properties of the spot emission pattern. *NICER* is using this approach to measure NS radii, based on the shape and amplitude of the pulsed emission observed from pulsar surface in multiple wavebands. The data accuracy allows for precise comparison between measurements and models of NSs (Sieniawska et al. 2018), and will significantly improve our understanding of the physics of superdense matter in the universe. Indeed, *NICER*'s X-ray data from PSR J0030+0451 has recently led to the first precise measurements (below 10% uncertainty) of the radius and mass of a pulsar (see Bilous et al. 2019; Bogdanov et al. 2019a, 2019b; Guillot et al. 2019; Miller et al. 2019; Raaijmakers et al. 2019; Riley et al. 2019). Besides, it has also allowed for the first map of the hot spots on the surface of a star. It provided the locations, shapes, sizes, and temperatures of the heated regions, which should give precise details of the magnetic field of a neutron star (NS). In this regard, it has already been found that the hot spots are far from antipodal, meaning that the magnetic field structure of a compact star is much more complex than previously thought.

In order to constrain uncertainties up to a few percent, stellar rotation should be large (>100 Hz), time resolution should be small ($\lesssim 10\ \mu$s), and the number of photons should be large (at least $\sim 10^6$; Watts 2019). However, it is still possible to obtain interesting constraints on the properties of slowly rotating NSs, such as the Soft Gamma Repeaters (SGRs) and the Anomalous X-ray Pulsars (AXPs).

SGR 1745-2900 was the first SGR detected near the Milky Way center, Sagittarius A* (Kennea et al. 2013; Mori et al. 2013), and it is at distance of 8.3 kpc. It has a rotational period

$P = 3.76$ s and a changing spindown rate since the 2013 outburst. From its latest update, it is $\dot{P} \sim 3 \times 10^{-11}$ s/s (Coti Zelati et al. 2017). It is characterized by an X-ray luminosity $L_X \approx 10^{32}$–10^{36} erg s^{-1}. Owing to the flaring/outburst activity (10^{38}–10^{45} erg), SGR 1745-2900 has been classified within the SGR and AXP class (see, e.g., Olausen & Kaspi 2014). For a comprehensive review on observations of SGR 1745-2900, even the long-term ones, see Coti Zelati et al. (2015, 2017). For a systematic study of pulsed fractions of magnetars in quiescent state, including SGR 1745-2900, see Hu et al. (2019).

In this paper, we apply the approach of Turolla & Nobili (2013) for the emission of an NS with hot spots to two X-ray light curves of SGR 1745-2900 in different epochs. We use Genetic Algorithm (GA) techniques to constrain the mass and radius of SGR 1745-2900 with a minimum set of assumptions. This paper is organized as follows. In Section 2, we present the aspects of the model used for obtaining light curves from NS surfaces with hot spots. Section 3 explains the genetic algorithm techniques we use for fits of the SGR 1745-2900 light curves and how to obtain the NS parameters. In Sections 4 and 6 we present our results and discuss them.

2. Pulsed Profile Model

Here we show how the theoretical pulsed profiles are calculated for an NS with thermal spots on its surface. We follow the procedure of Turolla & Nobili (2013) to calculate the observed flux, which allows us to treat circular spots having arbitrary size and location on the stellar surface. The mass and radius of the star are denoted by M and R, respectively, and the spacetime outside the star is described by the Schwarzschild metric, i.e., we neglect rotational effects. This is an accurate approximation for SGR J1754-2900 given its slow rotational period of 3.76 s (clearly contrasting with millisecond pulsars, see, e.g., Belvedere et al. 2015; Cipolletta et al. 2015; Coelho et al. 2017). Let (r, θ, ϕ) be a spherical coordinate system with the origin at the stellar center and the polar axis along the line of sight (LOS; see Figure 1).

We consider an observer at $r \rightarrow \infty$ and a photon that arises from the stellar surface at $dS = R^2 \sin\theta d\theta d\phi$, making an angle α with the local normal to the surface ($0 \leqslant \alpha \leqslant \pi/2$). The photon path is then bent by an additional angle β owing to the spacetime curvature, and the effective emission angle as seen by the observer is $\psi = \alpha + \beta$ (see Figure 1). The geometry is symmetric relative to ϕ. Beloborodov (2002) has shown that the following simple approximate formula can be used to relate the emission angle α to the angle θ:

$$1 - \cos\alpha = (1 - \cos\theta)\left(1 - \frac{R_s}{R}\right), \quad (1)$$

where $R_s = 2GM/c^2$ is the Schwarzschild radius and G denotes the gravitational constant. We note that Equation (1) is a very good approximation for $R > 3R_s$ since it typically leads to very small errors ($\lesssim 1\%$). For the range of masses and corresponding radii of interest here, errors would be up to a few percent.

We assume that the spot emission follows a local Planck spectrum and that the observed flux comes mainly from hot spots. The intensity $B_\nu(T)$ is given by a blackbody with temperature T, where ν is the photon frequency. The flux is proportional to the visible area of the emitting region (S_V) plus
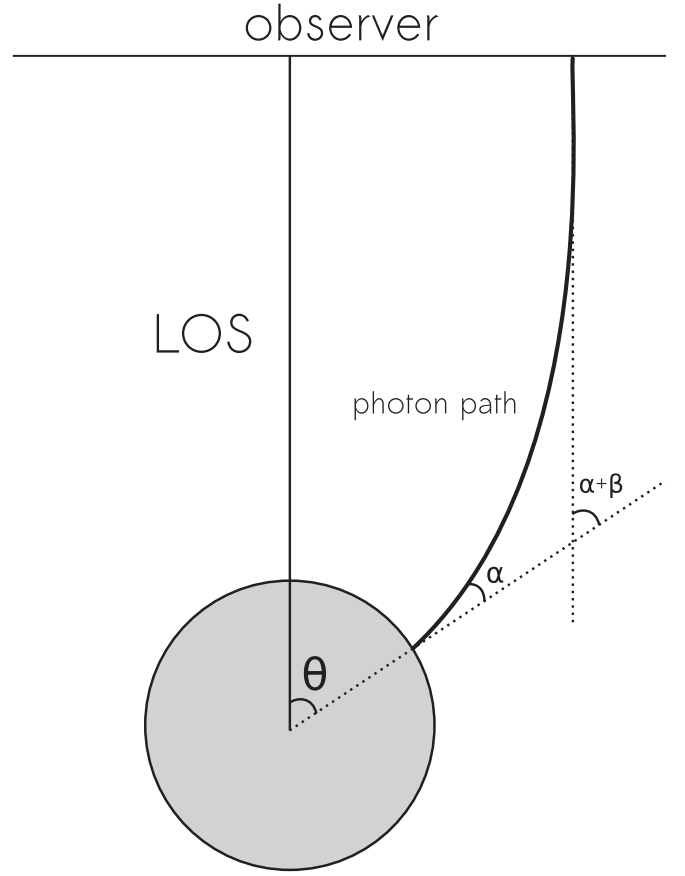

Figure 1. Illustration of the model geometry showing the photon trajectory and the angles θ, α, and β.

a relativistic correction, and it is given by (Beloborodov 2002; Turolla & Nobili 2013)

$$F_\nu = \left(1 - \frac{R_s}{R}\right)^2 B_\nu(T) \int_{S_V} \cos\alpha \frac{d\cos\alpha}{d(\cos\theta)} ds$$
$$= \left(1 - \frac{R_s}{R}\right)^2 B_\nu(T)(I_p + I_s), \quad (2)$$

where

$$I_p = \int_{S_V} \cos\theta \sin\theta d\theta d\phi, \quad I_s = \int_{S_V} \sin\theta d\theta d\phi. \quad (3)$$

In polar coordinates, the circular hot spot has its center at θ_0 and a semiaperture θ_c. The spot is bounded by the function $\phi_b(\theta)$, where $0 \leqslant \phi_b \leqslant \pi$, and since we must consider just the visible part of the star, the spot must be also limited by a constant θ_F. It is defined by

$$\theta_F = \arccos\left(1 - \frac{c^2 R}{2GM}\right)^{-1}. \quad (4)$$

For a given bending angle β, θ_F occurs for the maximum emission α, i.e., $\alpha = \pi/2$. In Newtonian gravity, where $\beta = 0$, the maximum visible angle is $\theta_F = \pi/2$, meaning that half of the stellar surface is visible. However, for a relativistic star

$\theta_F > \pi/2$. Then

$$I_p = 2 \int_{\theta_{\min}}^{\theta_{\max}} \cos\theta \sin\theta \phi_b(\theta) d\theta,$$

$$I_s = 2 \int_{\theta_{\min}}^{\theta_{\max}} \sin\theta \phi_b(\theta) d\theta, \qquad (5)$$

where $\theta_{\min}$, $\theta_{\max}$ are the limiting values, to be determined to the spot considered. Turolla & Nobili (2013) show how to solve these integrals and how to carefully treat the limiting angles. Finally, the flux given by Equation (2) can be written as (Turolla & Nobili 2013)

$$F_\nu = \left(1 - \frac{R_s}{R}\right)^2 \frac{B_\nu(T)}{D^2} A_{\text{eff}}(\theta_c, \theta_0), \qquad (6)$$

where D is the distance to the source, and it corrects the flux for an observer on Earth, and A_{eff} is the effective area, given by

$$A_{\text{eff}}(\theta_c, \theta_0) = R^2 \left[\frac{R_s}{R} I_s + \left(1 - \frac{R_s}{R}\right) I_p\right]. \qquad (7)$$

The total flux produced by N_σ spots, where the σth spot has a semiaperture $\theta_{c\sigma}$ and a temperature T_σ, can be calculated by adding up each contribution, and so we have

$$F_\nu^{\text{TOT}} = \left(1 - \frac{R_s}{R}\right)^2 \sum_\sigma \frac{B_\nu(T_\sigma)}{D^2} A_{\text{eff}}(\theta_{c\sigma}, \theta_{0\sigma}). \qquad (8)$$

Besides, the pulse profile in a given energy band $[\nu_1, \nu_2]$ for a given spot σ is

$$F_\sigma(\nu_1, \nu_2) = \left(1 - \frac{R_s}{R}\right)^2 A_{\text{eff}}(\theta_{c\sigma}, \theta_{0\sigma}) \int_{\nu_1}^{\nu_2} \frac{B_\nu(T_\sigma)}{D^2} d\nu. \qquad (9)$$

Therefore, one can rewrite Equation (8) for a given energy band, and it becomes

$$F^{\text{TOT}} = \sum_\sigma F_\sigma(\nu_1, \nu_2). \qquad (10)$$

We define by $\hat{r}$ the unit vector parallel to the rotation axis of the star, whose angular velocity is $\Omega = 2\pi/P$. It is also useful to introduce i, the angle between the LOS (unit vector $\hat{l}$) and the rotation axis, and j, the angle between the polar cap axis (unit vector $\hat{c}$) and the rotation axis ($\cos i = \hat{r} \cdot \hat{l}$ and $\cos j = \hat{r} \cdot \hat{c}$).

When the total flux, Equation (10), is calculated for a given configuration (i, j) for a time interval $(0 - P)$, the typical result is a pulsed flux with a maximum ($F_{\max}$) and a minimum flux ($F_{\min}$). We shall use the normalized version of Equation (10), given by

$$\bar{F}^{\text{TOT}} = \frac{1}{\bar{N}} F^{\text{TOT}}, \qquad (11)$$

where $\bar{N} = (F_{\max} + F_{\min})/2$. This normalization makes our model independent of the source distance, avoiding uncertainties linked to its precise determination. As SGR 1745-2900 is located near the Galactic center, its emission is heavily absorbed by the interstellar medium (ISM). However, we have verified that the ISM absorption can be neglected when using this normalization.

Table 1
List of Parameters and Ranges Used in Our Genetic Algorithm to Fit a Light-curve

Chromosome		
Gene	Definition	Range
$M(M_\odot)$	Star's mass	1.0–2.0
R (km)	Star's radius	8.9–13.7
N_σ	Number of hot spots	1–4
$\theta_{c\sigma}$	σth spot's semiaperture	2°–180°
T_σ (keV)	σth spot's temperature	0.0–0.9
θ_σ	σth spot's colatitude	0°–180°
ϕ_σ	σth spot's longitude	0°–360°
i	Angle between the LOS and the rotation axis	0°–90°
j	Angle between the polar cap and the rotation axis	0°–90°

We also define the pulsed fraction as

$$\text{PF} = \frac{F_{\max} - F_{\min}}{F_{\max} + F_{\min}}. \qquad (12)$$

We have considered two main physical scenarios. (i) Two-spot configuration: the spots can have any size and temperature, but their centers are diametrically opposed (as the poles of a dipolar magnetic field). So, in this case, the spots are called polar caps and we can define a polar cap axis. (ii) Three-spot configuration: two-spot configuration plus a third spot of any size, location, and temperature.

As the star rotates, the polar coordinate of the spot's center, θ_0, changes. Let $\gamma(t) = \Omega t$ be the star's rotational phase. Thus, from a geometrical reasoning we have that

$$\cos\theta_0(t) = \cos i \cos j - \sin i \sin j \cos\gamma(t), \qquad (13)$$

where we have taken that i and j do not change with time.

3. Genetic Algorithms

A GA is a type of programming technique inspired in the modern understanding of natural selection, i.e., the best genetic code is the one whose phenotype manages to survive all natural vicissitudes. In our work, the chromosome is given by the set of all free parameters used to generate a theoretical pulse profile. In GA, the individual parameters of a chromosome are called genes. In our case, the mass and radius of the star (M and R) and the angles i and j are examples of genes. The entire set of genes is given in Table 1.

The desired phenotype is given by the observed pulse profile, and a chromosome fitness is calculated from it. A typical GA procedure comprises six steps:

(1) Initialization: generation of a population of solutions (i.e., the chromosomes).
(2) Phenotype evaluation—calculation of each model solution fitness.
(3) Selection of the best solutions.
(4) Reproduction—the genes of the best solutions are recombined.
(5) Mutation—genes can be randomly selected and changed.
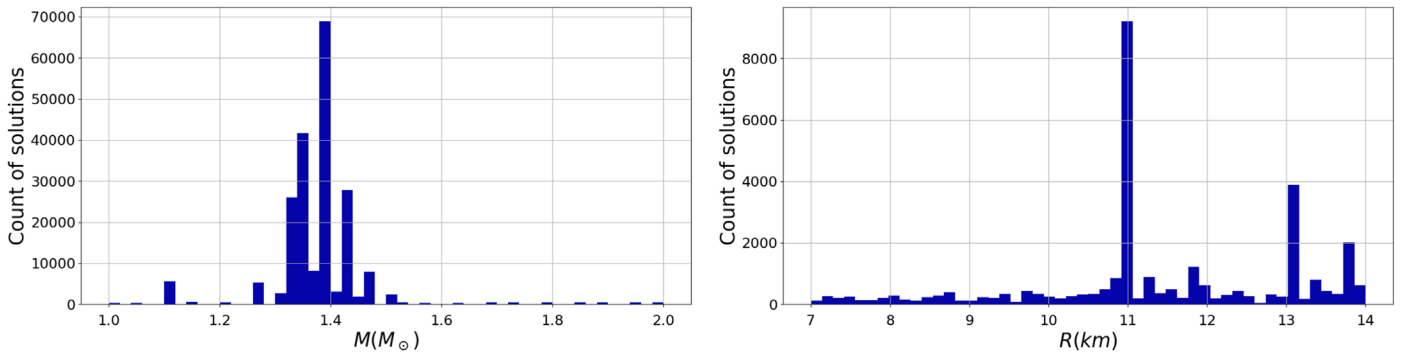(6) Population replacement.

Figure 2. Histograms of all generations of solutions for D13 and D16. Left panel: from a normal distribution fit of the count of solutions one learns that the mean mass is $1.4 M_\odot$ and the standard deviation is $0.1 M_\odot$. Right panel: the histogram shows the count of solutions of different radii for $M = 1.4\ M_\odot$ (the mean mass). Also from a normal distribution fit, the mean radius in this case is given by $R = 10.9$ km and the standard deviation is 1.5 km.

Every iteration from step 2 to 6 is called a generation. In order to handle the genetic evolution and gene operations, we use the python library Pyevolve,[12] maintained by Christian S. Perone and modified by us.

3.1. Goodness-of-fit Calculation

The goodness-of-fit (GoF) of a given solution is calculated by the square of the difference between the model and the observed data. This is summed over the period of the pulsed profile, i.e.,

$$\mathrm{GoF} = \sum_k [\bar{F}_k^{\mathrm{TOT}} - \bar{F}_k^{\mathrm{OBS}}]^2, \qquad (14)$$

where $\bar{F}_k^{\mathrm{TOT}}$ is given by Equation (11). Note that the summation is discrete because of the data nature, but the temporal change in $\bar{F}_k^{\mathrm{TOT}}$ is controlled by Equation (13) over the star's period. $\bar{F}_k^{\mathrm{OBS}}$ is the normalized observed flux and $k = 1$–N, where N is the number of observed points of the light curve. The optimal case would be GoF = 0. Therefore, the GA's goal is to minimize GoF. We note that the data uncertainty σ of SGR 1745-2900 is a given constant for each data set, and hence GoF and the standard χ^2 ($\chi^2 \equiv \mathrm{GoF}/\sigma^2$) carry the same statistical information. Since the definition given by Equation (14) is better suited for numerical computations, we use it for our fits. However, for statistical considerations we use χ^2 in order to be closer to standard analyses.

4. Results

Our aim is to find the set of parameters (see Table 1) that best fit the X-ray emission of SGR J1745-2900. We use the light curve from two epochs: 2013 (D13) and 2016 (D16)—presented by Coti Zelati et al. (2017). We let the parameters evolve as laid out in Section 3, and this is done independently for each data set. The final criterion to accept the best solutions is that both D13 and D16 result in the same most likely radius and inclination angles i and j, since these are expected to remain stable. For the determination of the mass and radius (based on the mean mass) ranges, global data analyses have been done, as explained below.

We have performed a "zeroth run" with all data points to find out which values of mass were the most likely to fit the SGR 1745-2900 light curve. This has been done in order to fix

one parameter and expedite the convergence time of subsequent (more precise) analyses. Our results are summarized in Figure 2 where one has the histogram of all generations of solutions fitting SGR 1745-2900 light curves. There one sees that, to one standard deviation, the majority of candidates have mass $1.4 \pm 0.1\ M_\odot$. Thus, we take the SGR 1745-2900 mass as a fixed value in the subsequent fits and equal to the mean value of the normal distribution of Figure 2, the canonical NS ($1.4 M_\odot$). However, as the large radius scattering of the zeroth run (when compared to the mass) already suggests ($R = 10.9 \pm 1.5$ km), we do not take the radius of SGR 1745-2900 as a fixed parameter in our subsequent investigations. Further details in this regard are given in Section 6.

As a first test, we have attempted to fit the light curve with only one hot spot, but the fits were very poor and are not discussed here. So we explore two spots, either having free positions or being antipodal. The two-spot fits can be seen in Figure 3 for the D13 data set, where the GoF per degree of freedom for the fits are in the range 0.041–0.044. In order to contemplate another geometry, we added a third hot spot with a free position relative to the other two, chosen to be antipodal. This choice of spots acts like a correction (which can be large) to the dipolar model, and, as shown below, it results in better fits to the light curves. A summary of the best-fit parameters for the D13 and D16 data sets in this case can be seen in Table 2. Figure 4 shows the best fits for the D13 and D16 sets using three spots. One can see that three spots fit reasonably well the main features of both data sets. For the D13 data set we find that GoF per degree of freedom is around 0.037, which is slightly better than the two-spot fits. We discuss further the quality of the fits and some subtleties of the D16 data set in Sections 4.1 and 6.

Figure 5 shows the hot spot positions on the stellar surface. The nonantipodal spot, in the southern hemisphere of the star, is responsible for the hottest blackbody temperature (0.87 keV) for both epochs, and its semiaperture increases from 2013 to 2016. This temperature is very close to 0.88 keV, as found by Coti Zelati et al. (2017) when fitting SGR 1745-2900 spectrum with a single hot spot.

4.1. Statistical Considerations

Given that some macroscopic aspects of the star should not change significantly from one period to the other, important conclusions could already be reached from one data set alone, for example D13. Clearly, three hot spots can fit better the data than two hot spots. This can be seen by their goodness-of-fit per degree
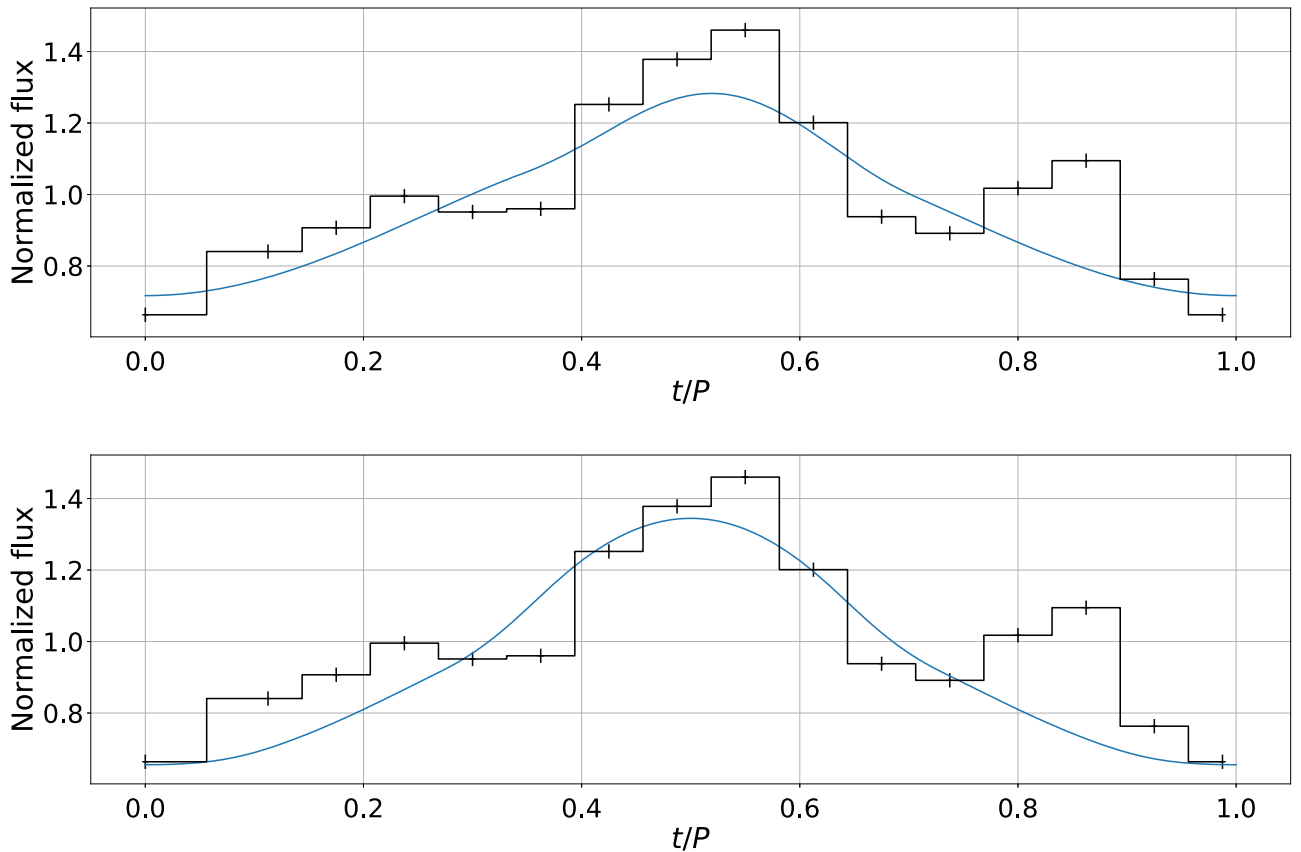
---

[12] http://pyevolve.sourceforge.net/

Figure 3. Upper panel: D13's fitting for two spots. The mass is 1.4 $M_\odot$ and the two spots are free. The radius found is $R = 13.74$ km, and GoF = 0.22. In this case, the number of degrees of freedom (DoF) is 5 and hence GoF/DoF = 0.044. Bottom panel: D13's fitting for two antipodal spots. The mass is 1.4 $M_\odot$, $R = 13.4$ km, and GoF = 0.29. Here, DoF = 7 and then GoF/DoF = 0.041. The normalization factor used in the plots is $\bar{N} = (F_{\max} + F_{\min})/2$.

Table 2
List of Solutions Found for D13 and D16

	Best Solutions	
	D13	D16
GoF	0.11	0.27
M ($M_\odot$)	1.40	1.40
R (km)	10.97	11.02
i	57°	58°
j	57°	56°
N_σ	3	3
PF	0.31	0.32
θ_{c1}	22°	40°
θ_1	0°	2°
ϕ_1	0°	351°
T_1 (keV)	0.6967	0.2857
θ_{c2}	16°	67°
θ_2	180°	178°
ϕ_2	0°	341°
T_2 (keV)	0.7858	0.0752
θ_{c3}	21°	26°
θ_3	102°	117°
ϕ_3	234°	225°
T_3 (keV)	0.8789	0.8798

Note. The positions of the spots can be visualized in Figure 5.

of freedom (GoF/DoF), as present in Figures 3 and 4 and in Table 3. However, for meaningful fit comparisons we calculate the standard reduced χ^2, $\chi^2_{\mathrm{red}} := \mathrm{GoF}/(\sigma^2 \mathrm{DoF}) = \chi^2/\mathrm{DoF}$ (σ is the

normalized error bar of the measurements). As is clear from Table 3, one can see that $\chi^2_{\mathrm{red}} = 2 - 6$ for both data sets. A possible interpretation of the large values of χ^2_{red} is an overfitting due to the small number of data points (resulting in a small DoF). We have also performed the F-test between nested models. The p-values of these statistics suggest that there is not a preferred model. This is not surprising given the large number of parameters when compared to the data (small number of degrees of freedom).

In order to increase the number of degrees of freedom, we have also attempted to fit the data in other ways. We have assumed the case where the D13 and D16 data sets are fit simultaneously for certain parameters. Our results are summarized in Table 4 (for free fitting masses and radii) and 5 (free fitting radii and fixed mass at 1.4 $M_\odot$). As one can clearly see, no case led to a preferred hot spot scenario. For instance, the χ^2_{red} found are as large as before, which is yet a consequence of the very small number of observational data for SGR 1745-2900. One might wonder what is the minimum amount of data points needed to reach more stringent results. As the goodnesses of fit of Table 4 already suggests, assume that this hypothesized case still leads to GoF ≈ 0.6 to the simultaneous fit. Then, it follows that $\chi^2_{\mathrm{red}} \approx 1.05$ would be reached when the degrees of freedom are approximately 70. This is much larger than our SGR 1745-2900 data. We come back to this issue in Section 6.

5. Additional Systematic Uncertainties to M and R

Care should be taken when extracting physical information from pure blackbody emission models. The processes
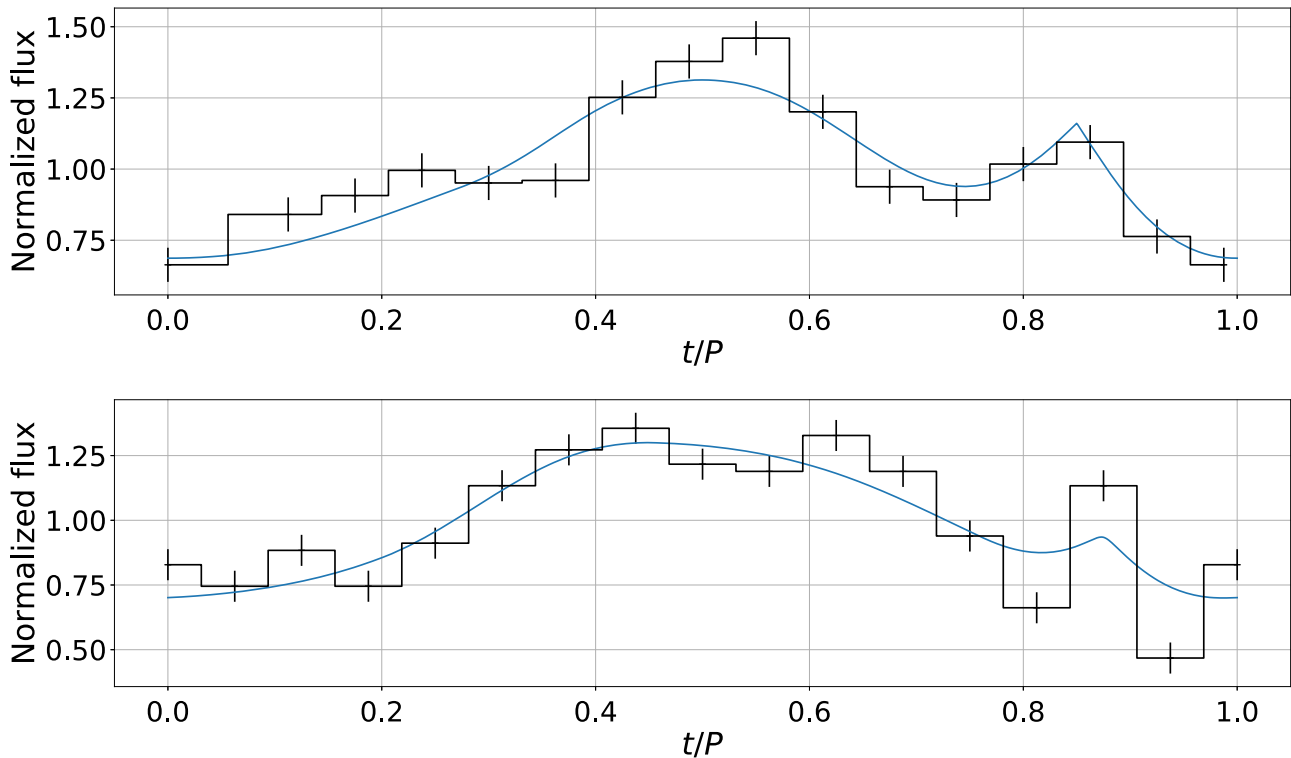
Figure 4. Upper panel: D13's fitting for three spots. The mass is 1.4 $M_\odot$ and two spots are antipodal, while the third one is free. The parameters found were $R = 10.97$ km, $j = 57°$, $i = 57°$, $T_1 = 0.6967$ keV, $T_2 = 0.7858$ keV, and $T_3 = 0.8789$ keV. GoF = 0.11 and the number of degrees of freedom here is 3 (the mass has been fixed by our zeroth run), which implies that GoF/DoF = 0.037. Bottom panel: D16's fitting for three spots. Same mass and spot configurations as the D13 set. The parameters found were $R = 11.02$ km, $j = 58°$, $i = 56°$, $T_1 = 0.2857$ keV, $T_2 = 0.0752$ keV, and $T_3 = 0.8798$ keV. GoF = 0.27 (GoF/DoF = 0.09).

responsible for radiation emission in SGRs/AXPs are still largely unknown. They may be related to the presence of an atmosphere, although with properties quite different from those of standard atmospheres around passively cooling NSs, or even arise from a condensed surface. In both cases, the spectrum is expected to be thermal but not necessarily blackbody-like (see, e.g., Potekhin 2014, and references therein). In the case of NSs, one can expect that the emitting layers are comprised of just one, lightest available, chemical element because heavier elements sink into deeper layers due to the immense NS gravitational field.

Several works have addressed the problem of modeling the radiation transport in magnetized NS atmospheres. Shibanov et al. (1992) were the first to perform detailed calculations of radiation spectra emerging from strongly magnetized NS photospheres, for the case of a fully ionized plasma. Besides, they have created a database of magnetic hydrogen spectra (see also Ho & Lai 2001; Ho et al. 2007, and references therein) and have shown that the spectra of magnetic hydrogen and helium atmospheres are softer than the nonmagnetic ones, but harder than the blackbody spectrum with the same temperature. Thus, if an amount of hydrogen is present in the outer layers (e.g., because of accretion of the interstellar matter), one can expect a pure hydrogen atmosphere. The latter can lead to much harder spectra in the Wien tail than the blackbody spectrum, because hotter deep layers are seen at high frequencies, where the spectral opacity is lower (Pavlov et al. 1996). In this case, the best-fit effective temperature of the atmosphere is considerably lower than the blackbody temperature, whereas the R/D ratio is larger than the one for the blackbody fit. Therefore, models that go beyond blackbody assumptions could have an important influence on SGR 1745-2900 mass and radius constraints.

A crude way of estimating further uncertainties to our M and R results due to the presence of atmospheres (e.g., hydrogen) could be as follows. One could average out the different hot spot temperatures in the D13 and D16 data sets and find a representative temperature and an uncertainty to them. With this uncertainty, one could estimate a range of wavelengths around the one for the maximum flux, λ_{max} (the most relevant wavelength for a given temperature), and then use known atmospheric models (Pons et al. 2007) to find the largest change of the flux (with respect to the blackbody) for this wavelength interval. Finally, by extrapolating these results, one gets the flux change estimates to our case. Using the spots' temperatures from Table 2, one has that a representative value for them is 0.6 ± 0.3 keV ($7.0 \pm 0.3 \times 10^6$ K).[13] For the above hot spot temperature uncertainty, one then expects the relevant wavelengths to range from $(2/3)\lambda_{max}$ to $2\lambda_{max}$. From Figure 6 of Ho et al. (2007; or Figure 1 of Suleimanov et al. 2009), it thus follows that hydrogen atmospheres of isolated magnetized stars should lead to a maximum difference in flux of approximately 20% when compared to blackbody results. If now one goes back to the expression of the flux and takes it as a function of M and R, it follows that a 20% change of it leads to a maximum uncertainty of approximately 7% to the radius and a 5% uncertainty to the mass with respect to blackbody outcomes. In order to reach these differences, we have taken

---

[13] If one assumes that the flux of the hot spots is around 10 times larger than the one from the star's surface (DeDeo et al. 2001), then the mean hot spot temperature should be around twice as large as the star's surface. This allows us to conclude that our fit parameters are in good agreement with independent fits of surface temperatures and magnetic fields of stars (Pons et al. 2007) since the surface dipolar magnetic field of SGR 1745-2900 would be around 2×10^{14} G (Coti Zelati et al. 2015).
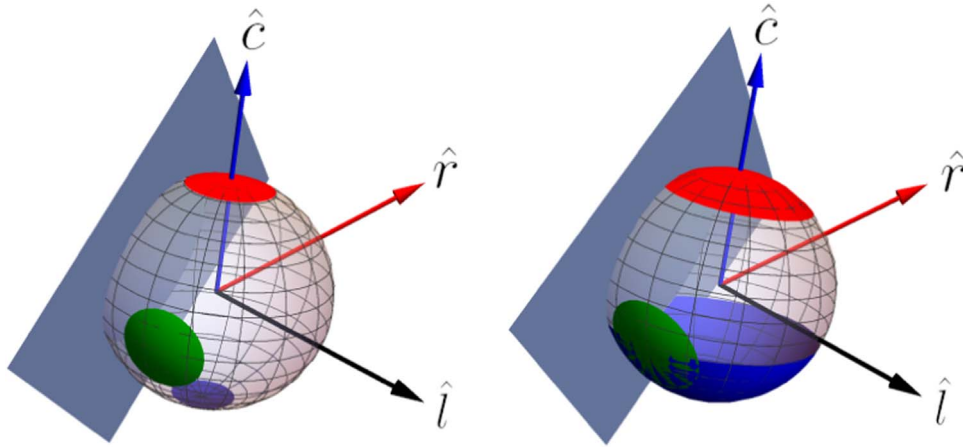
Figure 5. Left panel: D13's three-spot positions. $T_1 = 0.6967$ keV (north pole spot), $T_2 = 0.7858$ keV (south pole spot), and $T_3 = 0.8789$ keV (nonantipodal—or southern hemisphere—spot). Right panel: D16's three-spot positions. $T_1 = 0.2857$ keV (north pole spot), $T_2 = 0.0752$ keV (south pole spot), and $T_3 = 0.8798$ keV (nonantipodal spot). The arrows shown are the $\hat{l}$ (LOS), around the star's equatorial plane, $\hat{c}$ (polar cap axis), crossing the north pole, and $\hat{r}$ (rotation axis), the remaining arrow in the northern hemisphere. A plane is drawn as a reference to the maximum angle θ_F from which the observer cannot receive signals anymore.

Table 3
Acronym Meanings: Number of Fitting Parameters (NFP), Number of Data Points (NDP), and Degrees of Freedom (DoF)

		Separated Fits of D13 and D16 Epochs				
Model	A1	B1	C1	A2	B2	C2
Data	D13	D13	D13	D16	D16	D16
N_σ	2	2	3	2	2	3
Antipodal	y	n	y	y	n	y
GoF	0.29	0.22	0.11	0.33	0.35	0.27
σ	0.09	0.09	0.09	0.15	0.15	0.15
$\chi^2 (D_i)$	35.80	27.16	13.58	14.67	15.56	12.00
$\chi^2_{\rm red}$	5.11	5.43	4.53	2.10	3.11	4.00
NFP	9	11	13	9	11	13
NDP	16	16	16	16	16	16
DoF	7	5	3	7	5	3
Models	A1/B1	B1/C1	B2/C2			
F-statistics	0.7954	1.4999	0.4444			
p-value	0.5012	0.3535	0.6775			

Note. σ stands for the data uncertainty. The row "antipodal" specifies whether models have (y) or do not have (n) two antipodal spots. The F-statistics and p-value are calculated by comparing two models as indicated by $(X1)/(X2)$. The mean value of the mass has been fixed by the zeroth run, while the radii have been kept free for both epoch fits (see Section 4 for details).

$I_p = I_s \approx 0.015$ as a representative value. We note that the above changes could either increase or decrease the mean mass and radius of SGR 1745-2900 .

Another source of uncertainty to our blackbody-based results is light beaming. This is specially the case for systems with high magnetic fields (DeDeo et al. 2001; Suleimanov et al. 2009), as is very likely the case of SGR 1745-2900 (Coti Zelati et al. 2015). Besides the plasma present in the magnetosphere, the presence of an accretion column itself could lead the emission from hot spots to be beamed (DeDeo et al. 2001). When compared to isotropic emission models, beaming could change pulsed fractions substantially (DeDeo et al. 2001). One could crudely estimate additional uncertainties to our model in the following way. The averaged semiaperture angle from our hot spots is $\theta_c \approx 32°$ (see Table 2). From our model, the SGR 1745-2900 pulsed fraction is approximately 0.3.

Assuming that the hot spots could have a flux around 10 times larger than the star's surface (DeDeo et al. 2001), from Figure 4 of DeDeo et al. (2001), one sees that the most appropriate beaming index in this case should be $n = 1$ ($I \propto \cos^n \alpha$) and changes in the maximum to minimum flux ratio could be 65% (pulsed fraction going from 0.1, the maximum in the isotropic case (DeDeo et al. 2001), to 0.3, the inferred one from our analysis of SGR 1745-2900). This means, crudely speaking, that the flux could change around 30% from a pure blackbody. In terms of differences to macroscopic parameters, following the procedure laid out before for atmospheres, we find that beaming leads to a maximum difference of 6% to the mass and 10% to the radius. We stress that this is very model and parameter dependent and it is not excluded larger or smaller corrections to blackbody outcomes. We comment further on beaming in the discussion section.

All the above systematic uncertainties indicate that, so far, it is not possible to make predictions for the mass and radius of SGR 1745-2900 as precise as one would wish. Combining the above models, systematic modeling uncertainties could lead the radius and the mass to change by up to 20% and 10%, respectively. However, a clear aspect from our simple analysis is that fits with three hot spots resulted in smaller GoF, meaning that they are more statistically relevant than two hot spots. We discuss possible interpretations of that in the next section.

6. Discussions and Conclusions

Chandra X-ray data have been used to constrain SGR J1745-2900 properties by means of genetic algorithm techniques. From SGR 1745-2900 X-ray light curve and pulsed fraction and the assumption that they come from stellar hot spots of any size, temperature, and stellar position, fits have been made attempting to reproduce as best as possible the data. We took into account relativistic effects such as light bending and we have ignored the effects of stellar rotation, well supported by the SGR 1745-2900 long rotation period (3.76 s). In this first approach, we have also ignored atmospheric effects and beaming on the fits. Global and split into two epochs data have been investigated for uncertainty estimations and precise parameter extractions.

Although fits with three hot spots lead to better-than-two GoFs, statistical considerations have shown that both models

Table 4
The Mass and Radius Were Free to Vary and Have Been Simultaneously Adjusted for the D13 and D16 Epochs

	Simultaneous Fits of D13 and D16 with Free Masses and Radii							
Model	D		E		F		G	
Data	$D13 + D16$		$D13+D16$		$D13+D16$		$D13+D16$	
N_σ	2		2		3		3	
Antipodal	y		n		y		n	
GoF	0.5882		0.5589		0.5203		0.3761	
χ^2 (D13+D16)	45.21		42.71		39.28		19.05	
$\chi^2_{\rm red}$	2.83		3.56		4.91		4.76	
NFP	16		20		24		28	
NDP	32		32		32		32	
DoF	16		12		8		4	
D_i	D13	D16	D13	D16	D13	D16	D13	D16
GoF	0.2413	0.3469	0.2260	0.3329	0.2044	0.3159	0.0294	0.3467
σ	0.09	0.15	0.09	0.15	0.09	0.15	0.09	0.15
χ^2 (D_i)	29.79	15.42	27.91	14.80	25.24	14.04	3.64	15.41
Models	D/E	E/F	F/G					
F-statistics	0.1760	0.1746	1.0619					
p-value	0.9470	0.9452	0.4774					

Note. The intermediate GoF and χ^2 (D13 and D16) for the simultaneous fits are shown in the midpart of the table. The meaning of the acronyms and statistics are the same as in Table 3.

Table 5
The Meaning of the Acronyms Are the Same As in Table 3

	Simultaneous Fittings for D13 and D16. Stellar Mass Is Fixed at $1.4M_\odot$		
Model	H		I
Data	D13 + D16		D13 + D16
N_σ	2		3
Antipodal	y		y
GoF	0.5976		0.5272
χ^2 (D13+D16)	46.40		40.20
$\chi^2_{\rm red}$	2.73		4.47
NFP	15		23
NDP	32		32
DoF	17		9
D_i	D13	D16	D13	D16
GoF	0.2511	0.3465	0.2122	0.3150
σ	0.09	0.15	0.09	0.15
χ^2 (D_i)	31.00	15.40	26.20	14.00
Models	H/I		
F-statistics	0.1735		
p-value	0.9891		

Note. The middle part refers to the intermediate GoF and χ^2 for the simultaneous fits, as in Table 4.

are equivalent. This is due to the limitation of the observational data itself, which severely decreases the degrees of freedom of the system for the models. Even though the resultant statistics is poor in any case, one could interpret the above-mentioned ambiguity as a suggestion that a multipolar structure in SGR 1745-2900 should not be excluded. This comes from the fact that at least one model we have analyzed is a reasonable first-order description to NSs. Indeed, this should be the case for dipolar models since braking index measurements for pulsars are not too far from three (see, e.g., Coelho et al. 2016; de Araujo et al. 2016a, 2016b, 2016c, 2017) and some

properties of SGRs/AXPs would need strong dipolar fields (Coelho et al. 2017). Thus, if two hot spots are reasonable at the surfaces of stars and they are statistically equivalent to three hot spots, one should not disregard the latter (or other situations with more hot spots) in modeling NS light curves. This has indeed been shown to be the case of pulsar PSR J0030+0451, which strengthens even further the suggestions of our statistical analysis for SGR 1745-2900. We leave for future work investigations of light curves of NSs with more data points using the GA techniques developed here. In particular, we plan to investigate PSR J0030+0451, given that the hot spot configuration found for it is very different from what is expected in the dipolar case (see Bilous et al. 2019; Bogdanov et al. 2019a, 2019b; Guillot et al. 2019; Miller et al. 2019; Raaijmakers et al. 2019; Riley et al. 2019).

Regarding the normalized flux fits, some words are in order. First, we have not fitted both data sets entirely independently. We have taken the mean mass from our zeroth run (with all data sets run simultaneously; see Figure 2) in order to minimize the computation time of other parameters. This is reasonable because SGR 1745-2900 is an isolated NS. We have not taken the mean value of the radius from our zeroth run, but we have treated it as a free parameter in the D13 and D16 fits. However, we expect them, as well as the inclination angles i and j, to remain almost the same, as indeed happened to many populations, and that has been used as our criterion for selecting "the best" solution (see Table 2).[14] This shows consistency in our simple model. Nonetheless, the fit of the last points of the D16 data set indicates that the model is not entirely appropriate. This could be due to several reasons, one

---

[14] The GA we have made use of has a mutation parameter to prevent solutions from getting stuck in a false minimum. We have taken it to be 0.1, meaning that in every generation 10% of the population suffers mutation. Besides that, we have used many initial populations and have stopped running generations when the best solution (minimum of χ^2) had been the same for many successive generations (around 1000). Not all populations converged to the same solution, but we selected the physical one as the best of those with the same macroscopic parameters for both data sets.

of them being the small amount of data itself (see Coti Zelati et al. 2017). Another reason would be that we have modeled the data in a very simple way, forcing both epochs to be described equally, and important effects might have been left out. An example of that could be significant changes of SGR 1745-2900 atmospheric conditions from one epoch to the other. A sharp change of the beaming might also take place, meaning that accretion columns could change their properties due to an outburst. Indeed, it could rearrange or disturb the atmosphere of the magnetized NS, and as a result the flux could change non-negligibly. Thus, better fits could raise if different atmospheric models are taken for the epochs analyzed, which we have not done in this first analysis. We plan to elaborate on the above in future works.

The uncertainties to M and R, coming from our zeroth run, should be taken just as indicative. Systematic uncertainties due to different models could also be relevant. We have investigated some of them and it seems that atmospheric models and beaming could play an important role in more realistic uncertainties to the parameters. Rough estimates suggest that variations of the flux with respect to our model are around 50%, meaning an additional 20% (10%) radius (mass) uncertainty to SGR 1745-2900's mean blackbody outcomes. However, it is important to bear in mind that models for NS atmospheres are still debatable and blackbody results could give us interesting insights for testing them more precisely.

We now make a few comments regarding the case the surface of SGR 1745-2900 has three hot spots. The hot spots in Figure 5, in the light of the Gourgouliatos & Hollerbach (2017) results, could be interpreted as follows. First of all, the magnetic field at the stellar surface in both data sets seems to be far from axially symmetric because of the better fits coming from three hot spots. For the D13 set, the presence of the nonantipodal spot (southern hemisphere), whose size is comparable to the antipodal spots (north and south poles), suggests that the toroidal field should be relevant. Indeed, purely dipolar models would lead to spot areas of the order of the polar cap area $A_{pc} = \pi R_{pc}^2$, where $R_{pc} = \sqrt{2\pi R^3/(cP)}$ (see, e.g., Ruderman & Sutherland 1975; Cheng & Ruderman 1977; Chen & Ruderman 1993), and, for an NS with $R = 11$ km and $P = 3.76$ s, $A_{pc} \approx 0.023$ km^2, much smaller than the areas of the spots in Figure 5. This clearly indicates that the magnetic field of SGR J1754-2900 is very different from a dipolar configuration. According to Gourgouliatos & Hollerbach (2017), a very localized spot (≈ 1 km) implies a very specific configuration where 99% of the energy is in the toroidal field. However, smaller toroidal energy budgets lead to more extended magnetic zones at the stellar surface and, as a consequence, an extended hot region (Gourgouliatos & Hollerbach 2017). Therefore, our results suggest that SGR J1754-2900 has a complex multipolar magnetic field structure, with a relevant toroidal component for both D13 and D16 data sets (not overwhelmingly dominant, though, because the hot spots are not small). Indeed, the variability of the spindown rate of SGR J1745-2900 implies that its characteristic age (≈ 4.3 kyr) is accurate to its real age up to one order of magnitude, meaning it would be a young source and hence it might have a quite complex magnetic field structure. In addition, the association of some SGRs/AXPs with supernova remnants suggests that the ages of these sources are typically $\leqslant 10^4$–10^5 yr (see, e.g., Kaspi & Beloborodov 2017).

The variation of the spots' temperatures and sizes from one epoch to the other is pronounced. One might interpret these results as due to thermal conduction and temperature gradients on the stellar surface. This seems reasonable given the very large electric conductivity of the star, which would also imply a very large thermal conductivity, and so very small timescales for temperature variations. The temperature change of the spot at the north pole might be associated with its expansion, triggered by temperature gradients, and standard cooling processes. The significant temperature decrease of the south pole hot spot might also be due to its large increase, possibly triggered by similar reasons as to what happened to the north pole hot spot. However, the temperature change in the nonantipodal spot has been practically zero, and that might be related to its partial overlap with the south pole hot spot.

Apart from temperature values of some of the hot spots of SGR 1745-2900, our results contrast with those of Coti Zelati et al. (2017) for the same source and data. First, we have taken two and three hot spots, while they assume just a single one. Second, we have found that the sizes of the spots increase from 2013 to 2016, while the opposite happens to their single spot. In their case, the spot shrinking was important to explain the increase of the pulsed fraction. In our case, the increase of the pulsed fraction might be explained with the large temperature changes of some spots from one epoch to the other. Due to the relevance of hot spot size evolution to physical processes taking place in stars (Coti Zelati et al. 2017), we leave precise analyses thereof in light of our results to be carried out elsewhere.

We stress an important point of our analysis. One can see from the bottom panel of Figure 4 that our best fit to the normalized flux has not been so good for the last 2016 data points. This means that our pulsed fraction increase is not as pronounced (see Table 2) as the observed one (from approximately 0.35 to 0.58; Coti Zelati et al. 2017). We have tried to enhance the 2016 fit with three free hot spots on the stellar surface, but no better results have been found. Since in this case the number of free parameters is the same as the data points for each set, we have kept analyses with three hot spots where two of them are antipodal, which naturally have less parameters than data. Thus, it is still pending ways to enhance the fit of the last data points of the 2016 light curve of SGR 1745-2900.

We have performed a light curve and pulsed fraction X-ray data analysis of SGR 1745-2900 without assuming any specific nuclear EOS. The data analysis based on the blackbody model alone indicates that SGR J1745-2900 has as the most likely mass the canonical NS mass $M = 1.4 \, M_\odot$, and it should have a corresponding radius $R_{1.4} \approx 9.4$–12.3 km. This result obtained from electromagnetic data agrees with recent constraints obtained from gravitational wave observations that lead to $R_{1.4} \lesssim 13.5$ km for hadronic stars (Abbott et al. 2018; Annala et al. 2018; De et al. 2018; Most et al. 2018). The above values would disfavor relativistic mean-field theory models, which usually lead to $R_{1.4}$ larger than 13.5 km (Fortin et al. 2016). Some Skyrme models (see, for instance, Figure 7 of Fortin et al. 2016, where models should have $R_{1.4}$ in the range of 11.5–13.5 km), as well as the MPA1, APR, and WFF parameterizations (see their $R_{1.4}$ in Read et al. 2009), among other EOS, especially stiffer, seem to be favored by our analysis. However, the systematic modeling uncertainties that we have pointed out before significantly weaken the above

EOS constraints, and no definite conclusion can be reached so far; this might be mitigated just when precise emissions models are analyzed or when more data is collected. Finally, the question of whether SGR J1745-2900 could be a hybrid star remains open since many of the hybrid EOS would lead to a third family of NSs which would satisfy our light-curve constraints (see, for instance, Paschalidis et al. 2018; Sieniawska et al. 2019 and references therein).

Summing up, we have carried out fits of the light curve of SGR 1745-2900 using the genetic algorithm techniques. Although the observational data of SGR 1745-2900 is not enough to achieve stringent statistical conclusions, our analysis gave us important hints on magnetic fields of SGRs/AXPs. The fact that two or three hot spots could equally describe the data of SGR 1745-2900 suggests that in NS cases with more observations one should not disregard a multipolar structure of their magnetic fields.

ORCID iDs

Rafael C. R. de Lima ● https://orcid.org/0000-0003-1718-3838
Jaziel G. Coelho ● https://orcid.org/0000-0001-9386-1042
Jonas P. Pereira ● https://orcid.org/0000-0002-9385-5176
Claudia V. Rodrigues ● https://orcid.org/0000-0002-9459-043X
Jorge A. Rueda ● https://orcid.org/0000-0002-3455-3063

References

Abbott, B. P., Abbott, R., Abbott, T. D., et al. 2018, PhRvL, 121, 161101
Annala, E., Gorda, T., Kurkela, A., & Vuorinen, A. 2018, PhRvL, 120, 172703
Beloborodov, A. M. 2002, ApJL, 566, L85
Belvedere, R., Rueda, J. A., & Ruffini, R. 2015, ApJ, 799, 23
Bilous, A. V., Watts, A. L., Harding, A. K., et al. 2019, ApJL, 887, L23
Bogdanov, S., Guillot, S., Ray, P. S., et al. 2019a, ApJL, 887, L25
Bogdanov, S., Lamb, F. K., Mahmoodifar, S., et al. 2019b, ApJL, 887, L26
Chen, K., & Ruderman, M. 1993, ApJ, 402, 264
Cheng, A. F., & Ruderman, M. A. 1977, ApJ, 214, 598
Cipolletta, F., Cherubini, C., Filippi, S., Rueda, J. A., & Ruffini, R. 2015, PhRvD, 92, 023007
Coelho, J. G., Cáceres, D. L., de Lima, R. C. R., et al. 2017, A&A, 599, A87
Coelho, J. G., Pereira, J. P., & de Araujo, J. C. N. 2016, ApJ, 823, 97
Coti Zelati, F., Rea, N., Papitto, A., et al. 2015, MNRAS, 449, 2685
Coti Zelati, F., Rea, N., Turolla, R., et al. 2017, MNRAS, 471, 1819
de Araujo, J. C. N., Coelho, J. G., & Costa, C. A. 2016a, JCAP, 2016, 023
de Araujo, J. C. N., Coelho, J. G., & Costa, C. A. 2016b, ApJ, 831, 35
de Araujo, J. C. N., Coelho, J. G., & Costa, C. A. 2016c, EPJC, 76, 481
de Araujo, J. C. N., Coelho, J. G., & Costa, C. A. 2017, EPJC, 77, 350
DeDeo, S., Psaltis, D., & Narayan, R. 2001, ApJ, 559, 346
De, S., Finstad, D., Lattimer, J. M., et al. 2018, PhRvL, 121, 091102
Fortin, M., Providência, C., Raduta, A. R., et al. 2016, PhRvC, 94, 035804
Gendreau, K. C., Arzoumanian, Z., Adkins, P. W., et al. 2016, Proc. SPIE, 9905, 99051H
Gourgouliatos, K. N., & Hollerbach, R. 2017, ApJ, 852, 21
Guillot, S., Kerr, M., Ray, P. S., et al. 2019, ApJL, 887, L27
Ho, W. C. G., Kaplan, D. L., Chang, P., van Adelsberg, M., & Potekhin, A. Y. 2007, MNRAS, 375, 821
Ho, W. C. G., & Lai, D. 2001, MNRAS, 327, 1081
Hu, C.-P., Ng, C. Y., & Ho, W. C. G. 2019, MNRAS, 485, 4274
Kaspi, V. M., & Beloborodov, A. M. 2017, ARA&A, 55, 261
Kennea, J. A., Burrows, D. N., Kouveliotou, C., et al. 2013, ApJL, 770, L24
Miller, M. C., Lamb, F. K., Dittmann, A. J., et al. 2019, ApJL, 887, L24
Mori, K., Gotthelf, E. V., Zhang, S., et al. 2013, ApJL, 770, L23
Most, E. R., Weih, L. R., Rezzolla, L., & Schaffner-Bielich, J. 2018, PhRvL, 120, 261103
Olausen, S. A., & Kaspi, V. M. 2014, ApJS, 212, 6
Özel, F., & Freire, P. 2016, ARA&A, 54, 401
Özel, F., Psaltis, D., Arzoumanian, Z., Morsink, S., & Bauböck, M. 2016a, ApJ, 832, 92
Özel, F., Psaltis, D., Güver, T., et al. 2016b, ApJ, 820, 28
Paschalidis, V., Yagi, K., Alvarez-Castillo, D., Blaschke, D. B., & Sedrakian, A. 2018, PhRvD, 97, 084038
Pavlov, G. G., Zavlin, V. E., Truemper, J., & Neuhaeuser, R. 1996, ApJL, 472, L33
Pons, J. A., Link, B., Miralles, J. A., & Geppert, U. 2007, PhRvL, 98, 071101
Potekhin, A. Y. 2014, PhyU, 57, 735
Raaijmakers, G., Riley, T. E., Watts, A. L., et al. 2019, ApJL, 887, L22
Ray, P. S., Arzoumanian, Z., Brandt, S., et al. 2018, Proc. SPIE, 10699, 1069919
Read, J. S., Lackey, B. D., Owen, B. J., & Friedman, J. L. 2009, PhRvD, 79, 124032
Riley, T. E., Watts, A. L., Bogdanov, S., et al. 2019, ApJL, 887, L21
Ruderman, M. A., & Sutherland, P. G. 1975, ApJ, 196, 51
Shibanov, I. A., Zavlin, V. E., Pavlov, G. G., & Ventura, J. 1992, A&A, 266, 313
Sieniawska, M., Bejger, M., & Haskell, B. 2018, A&A, 616, A105
Sieniawska, M., Turczański, W., Bejger, M., & Zdunik, J. L. 2019, A&A, 622, A174
Suleimanov, V., Potekhin, A. Y., & Werner, K. 2009, A&A, 500, 891
Turolla, R., & Nobili, L. 2013, ApJ, 768, 147
Watts, A. L. 2019, in AIP Conf. Proc. 2127, Xiamen-CUSTIPEN Workshop on the EOS of Dense Neutron-Rich Matter in the Era of Gravitational Wave Astronomy, ed. A. Li, B.-A. Li, & F. Xu (Melville, NY: AIP), 020008
Zhang, S., Santangelo, A., Feroci, M., et al. 2019, SCPMA, 62, 29502